Journal of Catalysis 392 (2020) 197–208

Contents lists available at ScienceDirect

Journal of Catalysis

journal homepage: www.elsevier.com/locate/jcat

The application of inelastic neutron scattering to investigate iron-based Fischer-Tropsch to olefins catalysis

Alisha L. Davidson [a], Emma K. Gibson [a], Giannantonio Cibin [b], Hendrik van Rensburg [c], Stewart F. Parker [a,d], Paul B. Webb [e,*], David Lennon [a,*]

[a] School of Chemistry, Joseph Black Building, University of Glasgow, Glasgow G12 8QQ, UK
[b] Diamond Light Source, Harwell Science and Innovation Campus, Didcot OX11 0DE, UK
[c] Sasol Group Technology, 1 Klasie Havenga Street, PO Box 1183, Sasolburg 1947, South Africa
[d] ISIS Facility, STFC Rutherford Appleton Laboratory, Chilton, Didcot, Oxon OX11 0QX, UK
[e] School of Chemistry, Purdie Building, University of St Andrews, St Andrews KY16 9ST, UK

ARTICLE INFO

Article history:
Received 1 August 2020
Revised 22 September 2020
Accepted 23 September 2020
Available online 8 October 2020

Keywords:
Fischer-Tropsch-to-olefins catalysis
Inelastic neutron scattering
XANES
Chemical modifiers

ABSTRACT

The technique of inelastic neutron scattering (INS) is used to investigate how hydrogen is partitioned within a series of Na and S promoted iron-based Fischer-Tropsch-to-olefin catalysts. Two reaction test regimes are examined. First, reaction testing at elevated temperature and pressure demonstrate how Na/S additions enhance short chain olefin selectivity and reduce methane formation under industrially relevant reaction conditions. For a fixed level of Na incorporation (2000 ppm), sulfur concentrations of $\leq$ 100 ppm result in only a modest improvement in olefin selectivity. However, for sulfur values of $\geq$ 100 ppm there is a noticeable and systematic increase in C_2-C_4 olefin selectivity; rising from ~ 30.0% to 35.2% at 250 ppm. Second, using ambient pressure CO hydrogenation as a test reaction in INS and micro-reactor configurations, catalyst samples are further analysed by TPR, TPO, XRD and S K-edge XANES. INS shows the formation of a hydrocarbonaceous overlayer to be significantly attenuated by the presence of the promoters, with increasing S levels significantly reducing the intensity of the sp^2 and sp^3 hybridised ν (C-H) modes of the overlayer, albeit to differing degrees. A probable role for how this combination of promoters is perturbing the form of the hydrocarbonaceous overlayer to subsequently moderate the product distribution is considered.

1. Introduction

Short chain olefins (C_2-C_4) are high value platform chemicals used in the production of a diverse range of products including plastics, solvents, pharmaceuticals, synthetic textiles and cosmetics. Ethylene and propylene are among the highest production volume petrochemicals with long term projected growth periods driven by the needs of an ever-increasing global population [1]. Ethylene production is based mainly on steam cracking, a route that is dependent on finite, non-renewable sources of hydrocarbons [2]. In an era of heightened environmental awareness, alternative routes to chemicals and fuels from renewable feedstocks are under development and will play a central role in a future of sustainable chemical production and reduced carbon emissions. The transition towards a sustainable chemicals sector is in part responsible for the renaissance of Fischer-Tropsch (FT) technology, a process that provides a viable, alternative route to chemicals and fuels from biomass derived synthesis gas [2]. Commercial FT processes operating with Co-based catalysts target wax production, which is then hydrocracked to generate diesel. The product slate is highly paraffinic but chemicals, oxygenates and olefins, can be generated using Fe-based catalysts that display a lower, secondary hydrogenation activity [2,3]. Fischer-Tropsch product slates are typically broad in carbon number distribution and can be described by an Anderson-Schulz-Flory (ASF) model that is defined by the probability of chain growth, α. A maximum in C_2-C_4 yield is achieved with an α value of 0.4–0.5 but simply adopting strategies that reduce α, such as increasing reaction temperature, does not afford a viable route to light olefins owing to the concomitant increase in methane formation [2,4]. A commercially viable Fischer-Tropsch-to-olefin (FTO) technology, an area which has recently gained significant interest [4–17], must therefore

* Corresponding authors.
E-mail addresses: pbw@st-andrews.ac.uk (P.B. Webb), David.Lennon@glasgow.ac.uk (D. Lennon).

https://doi.org/10.1016/j.jcat.2020.09.025
0021-9517/

decouple C_1 and C_2-C_4 yields. A negative deviation from an ASF product slate can be achieved through the incorporation of promoter elements. Here, much effort has been dedicated specifically to the promotional effects of S and Na or K in Fe-based FT catalysts [4–13].

Alkali metals are used currently as promoters in commercially operated FT processes to achieve target activity [3,18]; they also provide selectivity benefits, such as reducing methane production and yielding a more chemical-rich product slate [3]. The origin of this shift in selectivity can be traced to enhanced activation of CO, which leads to an increased coverage of surface carbon relative to the supply of hydrogen [19]. An increase in the extent of carbidisation and carbon formation also occurs, which can again be rationalised by an enhancement of carbon supply and consideration of Niemantsverdriet's competition model [20,21].

Sulfur, on the other hand, is usually viewed as an FT catalyst poison, necessitating extensive clean-up of syngas feed in commercial operations [3,22,23]. At sufficiently low levels, however, a beneficial effect of sulfur is observed [6–8,18,24]. A study by Bromfield and Coville found a peak in catalytic activity and selectivity towards lower olefins upon the addition of *ca* 500 ppm of sulfur to an iron-based catalyst [18]. At higher concentrations of sulfur, the expected loss of catalytic activity occurred. The promotional effects of both Na and S have been exploited by Sasol in the development of an iron FTS catalyst that displayed high C_2–C_4 olefin selectivity (68% of olefins in the C_2–C_4 fraction), while simultaneously suppressing excess methane formation [25]. This enhancement in olefin selectivity has been confirmed in numerous studies [4–6,9,11] but definitive evidence for the origin of these selectivity benefits has not been provided to date. For example, Torres Galvis *et al.* [6] proposed that sulfur blocks hydrogenation sites, which inhibits chain growth termination via hydrogenation and favours the β-hydride abstraction pathway to unsaturated product [6]. Alternatively, Xie *et al.* consider how a Na/S promoter compound could change the binding geometry of the active iron carbide surface. This in turn is reported to decrease the availability of hydrogen atoms for the hydrogenation reactions that results in suppressed methane yields [26]. Recently, Paalanen and Weckhuysen have reviewed the role of Na/S promotion in iron-based FTS [11–13].

Product composition will be governed ultimately by the availability of surface intermediates and the precursors from which they are formed. Control of selectivity can therefore be achieved through the regulation of carbon and hydrogen supply within the catalytic system. Previously the authors have applied the technique of inelastic neutron scattering (INS) to investigate the potential role of a hydrocarbonaceous overlayer, that forms during Fe-catalysed FTS, in regulating the supply of hydrogen [27–33]. In this communication, the authors will explore how the addition of promoters S and Na affects the formation of the hydrocarbonaceous overlayer; correlating spectroscopic outcomes with the ability of the promoted catalysts to exhibit enhanced olefin production. INS is uniquely suited to the study of catalytic systems involving hydrogen owing to the anomalously high incoherent neutron scattering cross-section of ^{1}H (80. 3 barn) in comparison to other elements or isotopes typically relevant in catalysis (<5 barn). It is particularly well suited to testing real industrial based catalysts, which often cause significant challenges for conventional optical spectroscopy techniques such as infrared. This is due to the high absorption of IR radiation caused by the typically black colour and high metal loading of reacted catalysts. Supported catalysts may also lead to restrictions in the spectral range due to support cut-off effects. However, INS, unrestrained by the optical selection rules that regulate IR and Raman spectroscopies, overcomes these boundaries imposed from traditional optical spectroscopy, providing a means of detecting the vibrational modes of hydrogenous species over a wide spectral range (20–4000 cm^{-1}) [34]. The application of INS to probe catalysts has recently been reviewed by Albers and co-workers [34], whilst Parker *et al.* have reviewed recent technical advances for how certain configurations of established INS spectrometers can be applied to investigate novel aspects of heterogeneous catalysts utilised in a range of chemical transformations [35].

Against this background, the authors have recently used INS to investigate a series of iron catalysts promoted with sulfur alone [33]. Those preliminary studies show sulfur addition retards the reduction and carbidisation process of the hematite pre-catalyst, with a corresponding suppression of hydrocarbonaceous overlayer formation. In the current investigation, we expand on that initial INS study by examining the effects of incorporating a fixed concentration of sodium alongside varying levels of sulfur. The chosen levels of sulfur were influenced by the work of Bromfield and Coville (10 – 250 ppm) [18], with the sodium concentration kept constant at ~ 2000 ppm. These levels of sulfur are below that responsible for the maximum catalytic activity observed by Bromfield and Coville [18] but are comparable to other recent investigations [5,6]. The aim of this study is to determine how the tandem use of Na and S influences the CO hydrogenation surface chemistry over iron-based catalysts.

Reflecting the importance of hydrogen partitioning in FTS [27–32] and FTO [33] chemistry, inelastic neutron scattering is adopted as the principal investigative probe for the study. As considered elsewhere [28], the INS investigations utilise ambient pressure CO hydrogenation at elevated temperatures as the designated test reaction. This arrangement enables the surface chemistry of CO hydrogenation over iron-based catalysts to be examined without producing FTS products at the catalyst surface (*i.e.* long chain saturated hydrocarbons), which would otherwise dominate the resulting INS spectrum. Instead, ambient pressure CO hydrogenation favours methanation and water gas shift chemistry, with the products released into the gas phase. In this way, the INS spectrum provides information on the form of the catalyst [31], as well as hydrogen containing moieties that are retained at the catalyst surface [31,32]. Indeed, we postulate that these hydrogenous residues, in the form of a hydrocarbonaceous overlayer, are responsible for "templating" the actives sites [31]. The ambient pressure INS measurements undertaken at the ISIS Central Facility are backed up by laboratory micro-reactor measurements that enable reaction trends to be identified, as well as affording *in situ* post-reaction analysis in the form of temperature-programmed oxidation (TPO). It is readily conceded that none of the above constitutes actual FTS and/or FTO chemistry. Therefore, in order to assess how the hydrocarbonaceous overlayer may be linked to chemically moderated FTO activity, high pressure reaction testing representative of actual FTS/FTO reaction conditions is additionally undertaken. Collectively, the investigation shows how representative FTO catalyst formulations affect the formation of the hydrocarbonaceous overlayer, which is correlated with improved short chain (C_2-C_4) olefin selectivity and reduced methane production. Although the three-pronged approach (high pressure testing, ambient pressure INS and micro-reactor testing) provide a useful breadth in terms of perspective, it is acknowledged that the reaction conditions differ in each reactor, so that no single unifying reaction coordinate can be reasonably applied. Differences in advancement of the evolutionary phase of FTS chemistry between ambient pressure INS and micro-reactor measurements have been discussed elsewhere [28]. Nonetheless, this communication probes the molecular complexity inherent to FTO chemistry; a class of reaction with the potential to provide a new route to access low molecular weight olefins of direct importance to the petrochemicals industry.

2. Experimental

2.1. Catalyst preparation

The base iron oxide catalyst, hematite (α-Fe_2O_3) without promoters/modifiers (sample code **Fe-ref**), was prepared using the co-precipitation of iron nitrate (Sigma Aldrich, 99.99%) and sodium carbonate (Sigma Aldrich, 99.99%). Following precipitation, the slurry was filtered and washed with hot deionised water until the conductivity of the filtrate fell below 10 μS/cm. The precipitate was then calcined using a stepwise heating programme reaching a maximum temperature of 623 K. The procedure utilised a batch reactor apparatus for reproducible sample synthesis that is described elsewhere [30,31].

For the S/Na promoted samples, the filter cake obtained after washing was re-slurried in a small volume of water (*ca.* 40 ml) and precise quantities of the promoter elements added as ammonium sulfate and sodium carbonate dissolved in deionised water (20 ml). The sulfur levels were varied with intended values between 10 and 250 ppm, whereas the sodium levels were fixed at 2000 ppm. The modified samples were calcined using the same procedure as the un-promoted sample. All samples were ground and sieved to a particle size range of 250–500 μm. Sulfur and sodium content was quantified using inductively coupled plasma optical emission spectrometry (ICP-OES). Each of the promoted samples have been labelled **Fe-Na-S_x**, where the subscript × refers to the intended sulfur concentration in ppm. A sample containing only Na (sample code: **Fe-Na)** was prepared as a reference catalyst for use in the elevated temperature and pressure testing described in Section 3.2, in order to assist in establishing a role for sodium inclusion. The singly promoted Na sample was not available for ambient pressure INS or micro-reactor measurements.

2.2. Elevated pressure and temperature testing (FTO activity)

Catalyst testing was performed using a 4-fold parallel fixed bed reactor with an internal tube diameter of 6.5 mm. Product composition was determined by GC analysis of the 4 feed inlets and 4 product outlets using an Agilent Refinery Gas Analyser. The GC has two TCD channels, one for hydrogen and the other for permanent gases (CH_4, CO_2, Ar, N_2 and CO). A third FID channel analyses light organics (C_1-C_5). Product selectivities were calculated using Ar as an internal standard and based on CO conversion excluding CO to CO_2 production. Reaction conditions utilised here are comparable to those reported by Botes *et al.* [4]. 200 mg of catalyst, diluted in 3.2 g of SiC, was reduced *in situ* at 698 K under a flow of H_2 (40 ml/min) for 16 h at 20 barg, and cooled to 553 K. Once cooled, syngas was introduced (H_2/CO, 4:1, H_2: 100 ml/min, CO: 25 ml/min in carrier gas Ar: 15 ml/min; total weight hourly space velocity (WHSV) of 12.05 h^{-1}) and a temperature ramp at 0.5 K min^{-1} was used to reach reaction temperature of 603 K. Values quoted in Section 3.2 refer to product stream analysis performed after 6 h exposure to FTS conditions.

2.3. Micro-reactor measurements: Ambient pressure CO hydrogenation at 623 K

Most of the reaction testing was performed at ambient pressure using a catalyst test line composed of 1/8 in. diameter stainless steel Swagelok tubing, a description of which can be found elsewhere [30,31]. The catalyst was loaded into a 1/4 in. quartz tube reactor and plugged with quartz wool. The reactor is housed within a tube furnace (Carbolite MTF 10/15/30) equipped with PID control. A thermocouple is positioned within the catalyst bed to ensure accurate temperature readings during measurement. CO hydrogenation conditions were established over the bypass (CO: 3.91 ml min^{-1}, CK Gas, 99.8%; H_2: 7.93 ml min^{-1}, BOC Ltd, 99.8%; He: 24.0 ml min^{-1}, BOC Ltd, 99.9%) before introduction to the catalyst reactor (total WHSV of 13.63 h^{-1}). All gas flows were monitored using an in-line quadruple mass spectrometer (Hiden Analytical, HPR-20) that is attached to the reactor exit line via a differentially pumped, heated quartz capillary. Mass traces corresponding to sulfur compounds, *i.e.* hydrogen sulfide, sulfur monoxide and sulfur dioxide, were collected but all were below the instrument's detection limit during reaction testing. The sample was subjected to a temperature ramp of 5 K min^{-1} to 623 K and held for 6 h ; after which the reactant flows were halted and the temperature cooled to ambient temperature under the helium carrier gas. For *ex situ* characterisation, reacted samples were subjected to a passivation procedure involving a gradual increase in the oxygen levels up to atmospheric levels *(i.e.* 20% O_2 in the gas feed) [36]. Temperature programmed reduction (TPR) measurements are carried out on the micro-reactor set-up using hydrogen as the reductant in a 1:4 mix with helium (H_2: 10 ml min^{-1}; He: 40 ml min^{-1}).

2.4. In situ characterisation of post-reaction micro-reactor samples

Temperature-programmed oxidation studies of the micro-reactor samples were carried out post-reaction *in situ* on the micro-reactor catalyst test line described above. Previous TPO CO_2 measurements on unpromoted Fe FTS catalysts revealed three carbon peaks: α, β and γ, the assignments of which have recently been refined [32]. Oxygen (5% in He, 75 sccm, BOC Ltd, 99.5%) was introduced to the sample and the reactor heated to 1173 K at 5 K min^{-1} using the mass spectrometer to monitor the eluting gases (CO_2 and H_2O). The mass spectrometer response was calibrated for CO_2 [37] but not for H_2O. Various catalyst masses were assessed (20 – 40 mg) but, oddly, lower catalyst masses led to a loss of the CO_2 α peak. This carbonaceous feature is thought to be a key component in the formation of the hydrocarbonaceous overlayer, as well as contributing to the catalyst evolution process [32]. Thus, a larger catalyst mass of 40 mg was used for the TPO measurements of the doubly promoted samples to ensure this key component of the overall chemical transformations was observable. However, the larger catalyst mass led to increased quantities of retained carbon for the samples studied that exceeded the oxygen availability. Hence, the TPO profiles presented are qualitative rather than quantitative, as has previously been the case [28–33]. TPO profiles for **Fe-ref** originate from a previous series of measurements performed under comparable conditions [30].

2.5. Ex situ characterisation of micro-reactor samples

Ex situ powder X-ray diffraction (XRD) was performed using two separate instruments: both Panalytical X'Pert PRO MPD in the 2θ range 5 – 90°. One was equipped with a $Cu_{K\alpha}$ radiation and utilised for samples pre-reaction; the other is equipped with $Co_{K\alpha}$ radiation and used for post-reaction samples. The $Co_{K\alpha}$ was the preferred instrument for iron-based samples due to reduced fluorescence however, access was not readily available to this specific instrument which led to the dual approach adopted. BET N_2 physisorption measurements were performed on a Quadrasorb evo 3 BET station instrument, with overnight degassing of samples being carried out on a Quantachrome FloVac Degasser. Inductively coupled plasma-optical emission spectrometry (ICP-OES) measurements were performed by Butterworth Laboratories Ltd. The XANES data set was obtained at the Diamond Light Source located at the Rutherford Appleton Laboratory using the B18 beam line

measuring the sulfur K-edge using a QEXAFS setup with fast scanning Si (1 1 1) crystal monochromator. The incident beam intensity was monitored using a He-filled ionization chamber (Advanced Design Consulting Inc.) and the fluorescence signal measured using the SII Vortex 4-EM with Quantum detectors and XSPRESS3 readout electronics. The samples were ground in a pestle and mortar, stuck on to carbon tape and mounted into an automated sampler changer in the vacuum chamber. The raw data was processed in Athena, [38], based on the IFEFFIT library [39].

2.6. INS reactor measurements: Ambient pressure CO hydrogenation at 623 K

For INS measurements, approximately 10 g of catalyst was loaded into an Inconel reactor and attached to a custom-built sample preparation rig [40]. For ambient pressure CO hydrogenation measurements, the iron oxide catalyst was heated to 623 K at 5 K min^{-1} under a flow of CO (75 sccm, CK Gas, 99.9%) and H_2 (150 sccm, CK Gas, 99.9%) in a carrier gas (He, 600 sccm, CK Gas, 99.9%, total WHSV of 1.47 h^{-1}) and held at temperature for 8 h. The gas products were analysed by an in-line mass spectrometer (Hiden Analytical, HPR20 QMS Sampling System). Once the specific reaction had finished, the reactant gases were stopped, and the sample allowed to cool to room temperature under the carrier gas. The reactor cell was isolated and transferred to an argon-filled glove box (MBraun UniLab MB-20-G, [H_2O] < 1 ppm, [O_2] < 2 ppm) for loading into an aluminium sample holder that is sealed by an indium wire gasket [40]. All INS measurements were performed using the MAPS direct geometry spectrometer [35]. Spectra were recorded at 20 K at incident neutron energies of 650 and 250 meV using the A-chopper package. Quantification of the ν (C-H) feature obtained by INS was achieved following a calibration protocol described elsewhere [27–33,41].

2.7. Justification for reaction conditions adopted

The effect of how catalyst activation procedures may perturb post-reaction INS spectra has previously been considered [29] and has led to a standardised method for FT catalyst handling procedures suited to INS and micro-reactor measurements that includes a syngas reduction stage [30]. The work of Botes *et al.* was selected as a datum for an elevated pressure testing regime because it examined a suite of catalyst samples comparable to those under examination here that comprehensively reported C_2-C_4 olefin selectivity values [4]. However, that study included a CO_2 co-feed that was counter-balanced by a proportionally higher hydrogen ratio (H_2:CO = 4:1) compared to the more normal ratio of 2:1. In order to avoid further complications possibly originated from the CO_2 co-feed, this reagent was excluded from our elevated pressure measurements. A further deviation from procedures adopted by Botes *et al.* involved their use of a hydrogen reduction step. It is a non-trivial matter to combine bespoke spectroscopic measurements with directly comparable reaction testing procedures that additionally report specific and relevant outcomes. Nevertheless, the reaction conditions adopted here across the three disparate reaction formats (elevated pressure, ambient pressure micro-reactor and increased catalyst mass reactions for INS measurements) collectively provide a rigorous test for short chain olefin formation from a feedstream that might otherwise favour methanation. Thus, the adopted procedures define a hard test for olefin selectivity for the catalytic materials under inspection.

An additional variable to consider is the matter of reaction time. This is particularly pertinent to iron based FTS catalysts [2]. In a previous work, we have examined the unpromoted reference catalyst (**Fe-ref**) for CO hydrogenation activity for a period of up to 10 days [32]. That work clearly establishes that different phases of the catalyst conditioning process occur at different times. For complete equilibriation between the substrate and the vapour phase, reaction times of 100–200 h are required. However, in contrast, stabilised reaction profiles are observed from ~9 h T-o-S [32]. Thus, against this background, a reaction time of 6–8 h was selected as a suitable period of reaction that would be representative of key processes in FT surface chemistry. The elevated pressure measurements and the microreactor testing utilised 6 h T-o-S, whereas the INS measurements correspond to a reaction time of 8 h duration.

3. Results

The Results section is comprised as follows. Section 3.1 describes the physical characterisation of the five promoted pre-catalysts that are compared against an unpromoted iron oxide catalyst that has been previously investigated [30]. Section 3.2 reports on the outcome of elevated pressure FTS testing. An iron oxide sample singularly promoted with Na is also considered. INS measurements employ ambient pressure CO hydrogenation as a test reaction, so Section 3.3 presents ambient pressure test outcomes for the doubly promoted materials using a micro-reactor arrangement. Section 3.4 presents post-reaction characterisation of the microreactor samples (TPO and XRD). Section 3.5 uses XANES measurements to assess the S environment in the pre-catalysts and in post-reaction micro-reactor samples. Finally, Section 3.6 presents the INS measurements.

3.1. Catalyst characterisation

Before exposure to CO hydrogenation conditions, the promoted catalyst samples were characterised by ICP-OES, BET, XRD and TPR to establish whether the addition of the low levels of promoters, sulfur and sodium, had a significant effect on the structural and/or behavioural properties of the hematite pre-catalyst. Table 1 presents a combination of the ICP and BET data obtained for each of the doubly promoted catalysts alongside the reference material (**Fe-ref**) that was utilised in a previous study [31,32]. The sulfur concentrations used within this study are below reliable detection limits of ICP (<300 ppm) and, as such, are collectively banded as $\leq$ 100 ppm. However, the actual measurements are presented in parentheses and show a systematic increase in S levels across the samples that is in line with the intended values. As defined in Section 2.1, the addition of the sulfur to the base reference catalyst was a precisely controlled process, so the stated intended quantities should reflect the final composition of the catalyst. With the exception of **Fe-Na-$S_{100;}$**, the sodium concentration is within ± 10% of the intended target concentration. The excessive Na concentration for **Fe-Na-$S_{100;}$** is uniquely attributed to ineffective washing during the catalyst preparation stage for this sample. The surface area and pore volumes are comparable to the unpromoted reference catalyst, indicating the promoter addition process not to have noticeably affected the surface area or porosity of the samples. Attempts were made to additionally monitor sulfur inclusion by the application of electron energy loss spectroscopy within a high resolution analytical transmission electron microscope; the intention being to evaluate relative concentrations and spatial distributions. However, for all samples, the sulfur content was below the detection limit of the instrumentation.

Analysis of the promoted samples by XRD (Fig. 1) indicate reflections at 2θ = 24.4, 33.4, 35.9, 41.2, 49.7, 54.2, 57.8, 62.6, 64.2, 69.6, 72.1, 75.7, 80.8, 83.1, 85.2 and 88.9°, which are identical to the reference catalyst sample [30]. The observed reflections are characteristic of highly ordered hematite (α-Fe_2O_3); this establishes that the low levels of dual promotion are not perturbing

Table 1
Summary of ICP-OES and BET analysis of Fe-ref and the Na/S promoted catalysts (Fe-Na-S_x). BET measurements were performed in triplicate; standard deviation for surface area and pore volume are provided in brackets. Sulfur ICP-OES values are classified as ≤ 100 ppm, with the actual measurement obtained presented in parentheses.

Catalyst Sample	Sulfur ICP-OES Value (ppm)	Sodium ICP-OES Value (ppm)	Surface Area ($m^2\ g^{-1}$)	Pore Volume ($cm\ g^{-1}$)
Fe-ref	0	0	47.51 (*±3.21*)	0.230 (*±0.008*)
Fe-Na-S_{10}	<100 (*22*)	1855	45.44 (*±4.07*)	0.240 (*±0.011*)
Fe-Na-S_{50}	<100 (*41*)	2120	48.56 (*±0.662*)	0.265 (*±0.005*)
Fe-Na-S_{100}	<100 (*56*)	2890	47.36 (*±1.47*)	0.227 (*±0.028*)
Fe-Na-S_{175}	100 (*96*)	1910	47.89 (*±0.651*)	0.221 (*±0.004*)
Fe-Na-S_{250}	100 (*145*)	1820	46.14 (*±2.16*)	0.248 (*±0.004*)

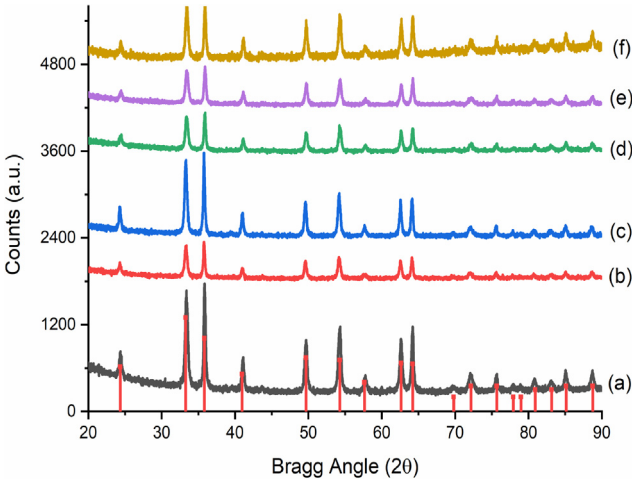

Fig. 1. X-ray diffractograms of (a) promoter-free α-Fe_2O_3 (Fe-ref) and promoted α-Fe_2O_3 (Na ~ 2000 ppm and varying sulfur concentrations (b) 10, (c) 50, (d) 100, (e) 175 and (f) 250 ppm S) of as-prepared catalysts. The red lines indicate reflections corresponding to the α-Fe_2O_3 reference diffractogram from the programme Highscore Plus. The diffractograms are vertically off-set for clarity.

the crystallinity or structure of the iron based FTS catalyst. Although the same reflections are seen for all samples, there is some variability in the intensity of the patterns; this is attributed to small differences in the mass of catalyst used in the individual measurements.

TPR studies were used to establish whether the inclusion of varying levels of sulfur alongside the fixed levels of sodium affected the reducibility of the catalyst (Fig. 2). The TPR profile for **Fe-ref** displayed two features at 597 and 779 K, corresponding to the reduction of hematite towards metallic iron via magnetite (*Equation (1)*) [29].

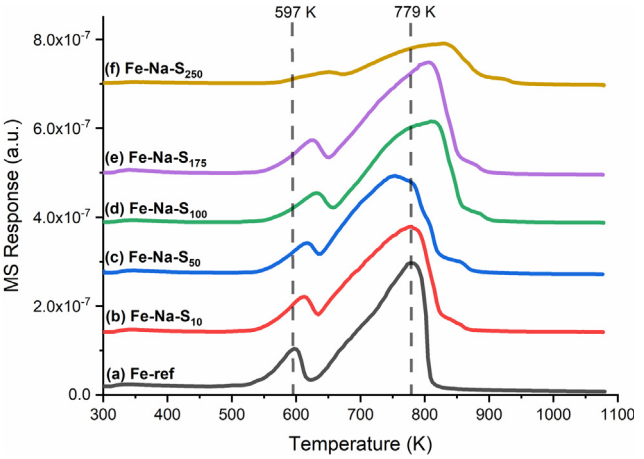

Fig. 2. In situ temperature programmed reduction profiles of (a) promoter free α-Fe_2O_3 (**Fe-ref**); (b) – (f) α-Fe_2O_3 with increasing levels of sulfur and a fixed Na content. The dashed lines indicate reduction events of the **Fe-ref** standard and highlight a shift in reduction to higher temperatures for the promoted samples. The profiles are vertically off-set for clarity.

$$\text{Hematite}(\alpha Fe_2O_3) \rightarrow \text{Magnetite}(Fe_3O_4) \rightarrow \text{Wüstite}(FeO) \rightarrow \alpha Fe \quad (1)$$

As the sulfur concentration is increased, these features shift to a higher temperature and for the highest sulfur sample (**Fe-Na-S_{250}**), the maxima of reduction events occur at 645 and 832 K (ΔT = 48 and 53 K respectively). This increase in T_{max} on increasing levels of S addition shows S to be retarding the reduction process associated with activation of the Fe_2O_3 pre-catalyst. The sole addition of S to iron-based FTS catalysts has previously been shown to impede formation of iron carbides during CO hydrogenation conditions [33].

3.2. Elevated pressure reaction testing (FTO activity)

Table 2 provides a comparison of the catalytic data of **Fe-ref**, **Fe-Na** and the S/Na promoted samples (**Fe-Na-S_x**) following exposure to the elevated temperature and pressure FTS conditions that closely correspond to those adopted by Botes *et al.* [4]. The data correspond to activity measurements for 6 h T-o-S at 603 K, where FT activity is based on CO conversion that excludes CO → CO_2 production. The reference catalyst exhibits representative FTS chemistry, with its activity noticeably higher compared to ambient pressure CO hydrogenation at 623 K [28–33], demonstrating the requirement of higher operating pressures to induce FTS activity. Moreover, the product slate is characterised by high levels of methane production alongside a range of predominantly paraffinic products. The addition of only sodium (**Fe-Na**) to the catalyst yields a favourable shift in selectivity to olefins as well as the desired reduction in methane production. This correlates well with literature precedent on the role of alkali metals in FTS [3]. The combination of both sodium and sulfur has been shown to further enhance selectivity to lower olefins while maintaining a low methane selectivity [4,6]. Fig. 3 presents the C_2-C_4 total olefin selectivity as a function of sulfur concentration. Low sulfur concentrations (≤100 ppm) result in only a modest improvement in olefin selectivity, however, for sulfur values of ≥ 100 ppm there is a noticeable and systematic increase in low molecular weight olefin selectivity; rising from ~ 30% to 35.2% at 250 ppm. Moreover, this trend is experienced within a regime of constrained methane production (Table 2). Interestingly, Table 2 shows the systematic increase in reduction temperature evident in Fig. 2 correlates with a comparable trend in olefin selectivity. It is noted that as the catalysts experienced different activation procedures for the TPR microreactor measurements (use of syngas as reductant) and the elevated pressure reaction testing (use of hydrogen as reductant), some caution is required in making such correlations. Nevertheless, such a comparison does indicate that S-induced impeded reduction profiles appear to be associated with favourable FTO product distributions. This issue will be revisited in **Section 4**.

Table 2
Selectivity data of catalysts exposed to FTS conditions (20 bar, 4:1 H_2:CO, T = 603 K) for 6 h T-o-S. The C_2-C_4 and C_{5+} classifications correspond to saturated and unsaturated products. FT activity is based on CO conversion that excludes CO → CO_2 production. The errors correspond to variation in the individual measurements as determined from a series of repeat measurements over a standard (unspecified) reference catalyst.

Sample	FT [μmol/g/s]	CH_4 (%)	CO_2 (%)	C_2-C_4 (%)	C_{5+} (%)	C_2 olefin:paraffin	C_3 olefin:paraffin	C_4 olefin:paraffin
Fe-ref	78.5 ± 3.9	24.9 ± 1.2	26.2 ± 1.3	41.8 ± 2.1	33.3 ± 1.7	0.1 ± 0.01	0.8 ± 0.04	1.3 ± 0.1
Fe-Na-S_{10}	55.5 ± 2.8	10 ± 0.5	34.2 ± 1.7	34.5 ± 1.7	55.5 ± 2.8	6.9 ± 0.4	8.3 ± 0.4	7.5 ± 0.4
Fe-Na-S_{50}	49.8 ± 2.5	9.6 ± 0.5	33.1 ± 1.7	34.3 ± 1.7	56.1 ± 2.8	7.6 ± 0.4	8.5 ± 0.4	7.6 ± 0.4
Fe-Na-S_{100}	47.9 ± 2.4	9 ± 0.5	33.6 ± 1.7	34.2 ± 1.7	56.8 ± 2.8	8.1 ± 0.4	8.7 ± 0.5	7.8 ± 0.4
Fe-Na-S_{175}	49.8 ± 2.5	8.8 ± 0.4	35.0 ± 1.8	35.4 ± 1.8	55.8 ± 2.8	7.9 ± 0.4	8.6 ± 0.5	7.8 ± 0.4
Fe-Na-S_{250}	47.9 ± 2.4	9.5 ± 0.5	34.4 ± 1.7	39.2 ± 2.0	51.3 ± 2.6	7.5 ± 0.4	8.9 ± 0.5	8.0 ± 0.4
Fe-Na	45.3 ± 2.3	10.6 ± 0.5	34.0 ± 1.7	33.7 ± 1.7	55.7 ± 2.8	7.5 ± 0.4	8.0 ± 0.4	7.3 ± 0.4

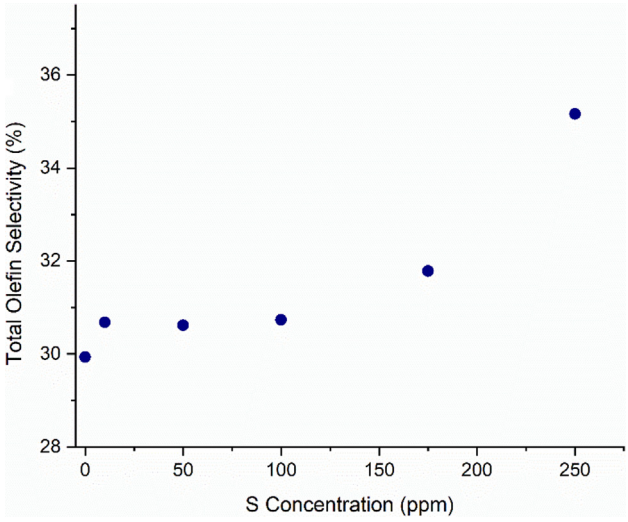

Fig. 3. Total olefin selectivity (C_2-C_4) of catalysts exposed to FTS conditions (20 bar, 4:1 H_2:CO, T = 603 K) for 6 h in relation to the S concentration (ppm) of each sample.

3.3. Micro-reactor: Ambient pressure CO hydrogenation reaction profiles

CO hydrogenation at ambient pressure and elevated temperature (623 K) was used as a test reaction to discern the performance of the doubly promoted iron samples. Reaction profiles were examined for a period of 6 h T-o-S. Fig. 4 presents reaction profiles of the samples containing the lowest (**Fe-Na-S_{10}**, Fig. 4a) and highest (**Fe-Na-S_{250}**, Fig. 4b) sulfur concentrations. Fig. S1 presents the extended dataset, *i.e.* [S] = 10–250 ppm. In addition to reactants and products normally analysed by mass spectrometry for a CO hydrogenation reaction, masses corresponding to sulfur monoxide (SO, *m*/*z* 48), sulfur dioxide (SO_2, *m*/*z* 64) and hydrogen sulfide (H_2S, *m*/*z* 34) were also monitored, but not observed, and are therefore not included in the profiles displayed. However, it is noted that on removal of the promoted samples from the reactor, a yellow staining was present on the quartz reactor tube that was not observed for **Fe-ref,** suggesting reaction induces the loss of S-containing moieties from the doped samples. (No staining or detection of sulfurous odours were apparent for the high pressure testing measurements.)

The reaction profiles of the promoted samples are comparable to that of the unpromoted catalyst, **Fe-ref** [30/33], displaying three distinct stages that are assigned as follows: *Stage I,* the reduction of α-Fe_2O_3 towards Fe_3O_4 identified by the onset of CO consumption and concomitant production of CO_2 at 515 K; *Stage II*, the simultaneous production of CO_2, H_2O and CH_4 from CO and H_2 at 623 K; *Stage III* represents steady state operation. Iron time yield (FTY) values for **Fe-Na-S_{10}** and **Fe-Na-S_{250}**, are 1.23×10^{-4} and 9.40×10^{-5} mmol (CO) $g_{Fe}^{-1}s^{-1}$ respectively, which is comparable to previously reported rates using similar reaction conditions [6]. Fig. 4**b** shows the highest sulfur loaded sample (**Fe-Na-S_{250}**) to display a prolonged production of CO_2. This is thought to be associated with increasing S concentrations impeding reduction of the Fe_2O_3 matrix and possibly sustaining water gas shift rates, as illustrated in Fig. 2.

3.4. Post-reaction characterisation, ambient pressure CO hydrogenation at 623 K (micro-reactor)

Recent work from the authors has examined TPO profiles for the iron reference catalyst (**Fe-ref**) that has been exposed to elevated

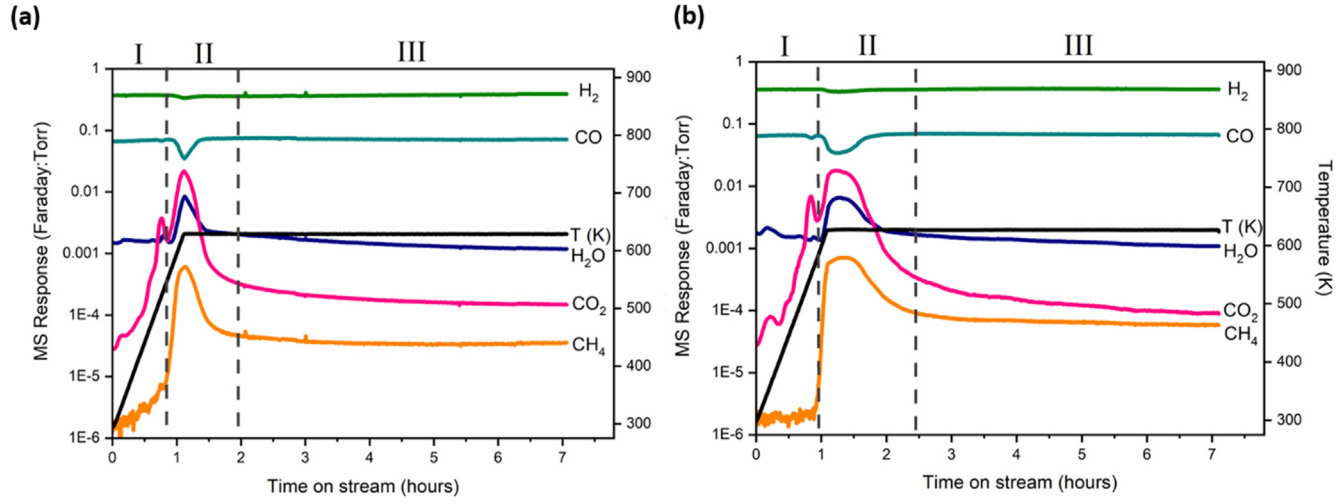

Fig. 4. Micro-reactor reaction profiles of with doubly promoted catalysts, a) 10 ppm & b) 250 ppm of S and a fixed level of Na (2000 ppm) during CO hydrogenation at ambient pressure and 623 K for 6 h T-o-S.

temperature, ambient pressure CO hydrogenation for up to 10 days T-o-S that required some refinement of assignments of retained carbonaceous entities [32]. Three distinct peaks were observed and are assigned as follows: Peak α is a low temperature feature associated with reactive carbon; Peak β is a medium temperature band that is associated with amorphous carbon; Peak γ is a high temperature feature that is attributed to signifying the presence of iron carbides as well as a contribution from polyaromatic carbonaceous species [32].

Fig. 5 presents the post-reaction TPO profile for Fe-Na-S_{250}, showing the oxygen consumption trace alongside the signals for CO_2 and H_2O. The former accounts for oxidation of retained carbonaceous species, whilst the latter is associated with oxidation of retained hydrogenous species. As described in Section 2.4, the TPO profiles are qualitative rather than quantitative. Fig. 5 shows the CO_2 signal to dwarf the H_2O signal, indicating the predominance of retained carbonaceous entities after 6 h T-o-S. Indeed, as indicated by the oxygen trace, the modifiers have caused such an increase in carbon bearing entities that they exceed the oxygen availability. This was not the case for unpromoted samples [30] and is thought to be a consequence of Na promotion. Accepting these outcomes, Fig. 6**(I)** shows a series of stack plots for the TPO CO_2 signal for the doubly promoted samples, whilst Fig. 6**(II)** represents a comparable plot for the TPO H_2O profiles.

Concentrating first on the retained carbon species (Fig. 6**(I)**), three peaks described above labelled α, β and γ are discernible [32]. Based on reaction trends, the TPO carbon α species is thought to be a precursor to formation of carbon-containing species including the aliphatic component of the hydrocarbonaceous overlayer, iron carbides and hard carbon [32]. Thus, it is a key component in the genesis of the active phase of the catalyst. For the unpromoted FTS catalyst (**Fe-ref**) it is a transitive species. From a previous study [32], Fig. S2 presents quantitative CO_2 profiles from post-reaction TPO microreactor measurements on **Fe-ref** that show the α carbon signal to increase on commencement of reaction up to a maximum value at approximately T-o-S = 24 h. Thereafter, its intensity decreases sharply, returning to baseline levels at T-o-S = 48 h [32].

Concerning relative intensities at T-o-S = 6 h for Fe-ref, the α peak is minor to the β peak [31]. Thus, the α peak prominence in Fig. 6, as indicated by the CO_2 signal but also by substantial oxygen consumption, implies that the presence of the Na and S are impeding aspects of the catalyst evolutionary process. With reference to Fig. 2, specifically this is thought to be via impairment of the catalyst reduction rate. Fig. 6 also shows the β peak, assigned to amorphous carbon [32], to increase on increasing levels of S.

Reverting to retained hydrogenous species, Fig. 5 shows the minimal water trace to exhibit features that correspond to the carbon α and β peaks, whilst Fig. 6**(II)** shows a trend of slowly increasing water signal on increasing levels of S promotion. Fig. 6**(II)** does reveal a hydrogen derived feature that has some correspondence with the γ peak of Fig. 5 that, converse to the α and β trends, tends to diminish on increasing S. The inter-dependence of the TPO data will be examined further in Section 4.

The *ex situ* XRD patterns of materials that have been exposed to CO hydrogenation conditions in a microreactor for 6 h T-o-S are shown in Fig. 7. The pattern observed for the reference catalyst (**Fe-ref**), assigned to Hägg carbide [30], is replicated for all the Na/S promoted samples. This indicates that over the 6 h timescale the dual promotion of Na and S is not constraining iron carbide formation in the micro-reactor, that itself reflects a component of the catalyst conditioning process [31,32]. However, as Table 2 and Fig. 3 show distinct trends concerning olefin selectivity for this range of materials, it is deduced that the XRD pattern alone does not display the characteristics that imbue olefin selectivity.

3.5. XANES S measurements

S K-edge XANES measurements were performed on the five doubly promoted pre-catalysts and on the same samples after ambient pressure CO hydrogenation in the micro-reactor (Section 3.3). The spectra were analysed with respect to literature peak positions of the following reference compounds: S, Na_2SO_3, $Na_2S_2O_3$, $FeSO_4$, and FeS_2 [42,43], as indicated in Table 3.

XANES spectra of the doubly promoted samples before reaction are shown in Fig. 8, with the sample containing the lowest sulfur concentration (**Fe-Na-S_{10}**) presented as an insert on a more sensitive y axis owing to the comparatively low signal intensity. All spectra are indicative of sulfur present in the form of sulfate, *i.e.* S^{6+}. This is to be expected as sulfur is incorporated into the catalyst using ammonium sulfate as the S precursor (Section 2.1). It is noted that materials with the lower levels of incorporated sulfur, **Fe-Na-$S_{10/50}$**, exhibit a feature at 2473 eV, corresponding to S^0 (Table 3). This species is also just discernible at 100 ppm. The origins of this partial and selective reduction of incident sulfur at the lower loadings is unknown.

After exposure to ambient pressure CO hydrogenation for 6 h in the micro-reactor at 623 K there are noticeable changes in the sulfur oxidation state (Fig. 9). Despite the poor signal:noise ratio in comparison to the untreated samples (thought to be due to the loss of S from the samples upon reaction testing, see Section 3.3), features are clearly discernible at 2471, 2473, 2481 and 2483 eV. The absorption at 2483 eV is also observed in the pre-catalysts (Fig. 8) and, with reference to Table 3, is assigned to S^{6+}, indicating that not all the sulfur within the catalyst is reduced under these reaction conditions. However, the lower energy peaks provide evidence of a sulfur reduction process (Table 3) [44]: the peak at 2481 eV corresponds to sulfur in the + 4 oxidation state (S^{4+}) and the two features at 2473 and 2471 eV are indicative of sulfur in 0 and −2 oxidation states respectively. Thus, following reaction, there is a range of S oxidation states present, suggestive of a step-wise reduction process from $S^{6+} \rightarrow S^{2-}$. This evident drive to forming a sulfide ion (S^{2-}) under reaction conditions may relate to the benefits of co-promotion. Bromfeld and Coville, using XPS to examine sulfur promotion of iron-based FTS catalysts, report a range of S oxidation states, the distribution of which are dependent on concentration and sample thermal history [45]. Further work by these authors establish the relevance of S^{2-} species to favourable FTS activity [18].

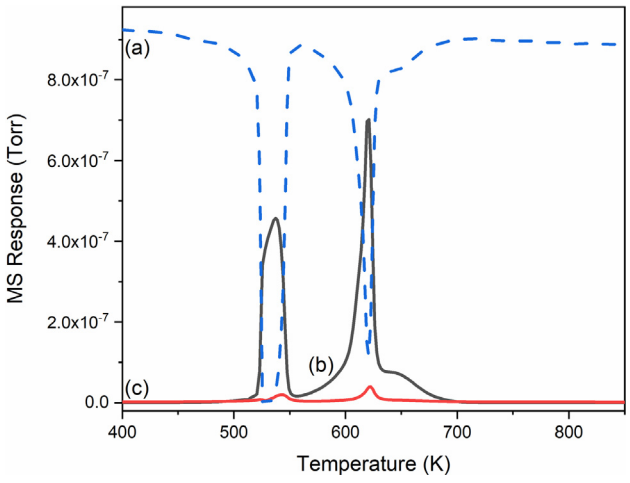

Fig. 5. In situ temperature programmed oxidation profile for Fe-Na-S_{250} after exposure to CO hydrogenation conditions at 623 K for 6 h in the micro-reactor: (a) oxygen consumption trace (blue), (b) CO_2 signal (black), (c) H_2O signal (red).

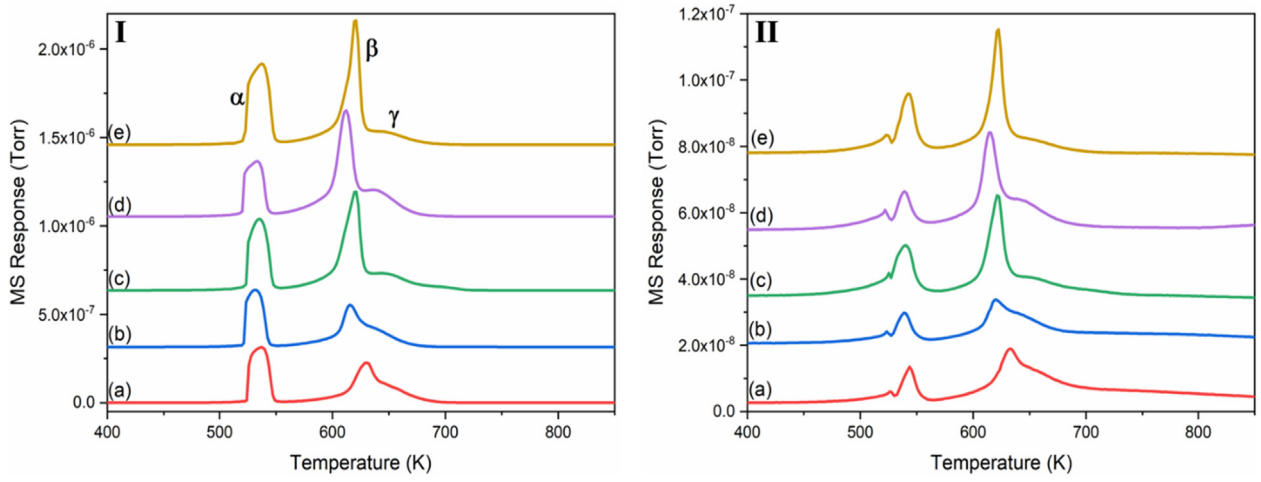

Fig. 6. *In situ* temperature programmed oxidation profiles. [**I** CO_2, **II** H_2O] of doubly promoted α-Fe_2O_3 with a fixed sodium concentration (2000 ppm) and varying sulfur concentrations (a) 10, (b) 50 (c) 100 (d) 175 and (e) 250 ppm after exposure to CO hydrogenation conditions at 623 K for 6 h in the micro-reactor. The profiles are vertically off-set for clarity.

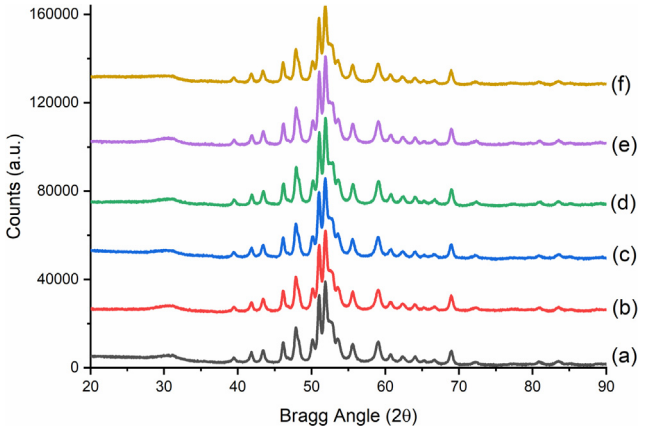

Fig. 7. X-ray diffractograms of (a) promoter-free α-Fe_2O_3 (Fe-ref) and Na/S promoted α-Fe_2O_3 (Na 2000 ppm and varying sulfur concentrations (b) 10, (c) 50, (d) 100, (e) 175 and (f) 250 ppm) of catalysts after exposure to CO hydrogenation conditions at 623 K in the micro-reactor set-up for 6 h. The diffractograms are vertically off-set for clarity.

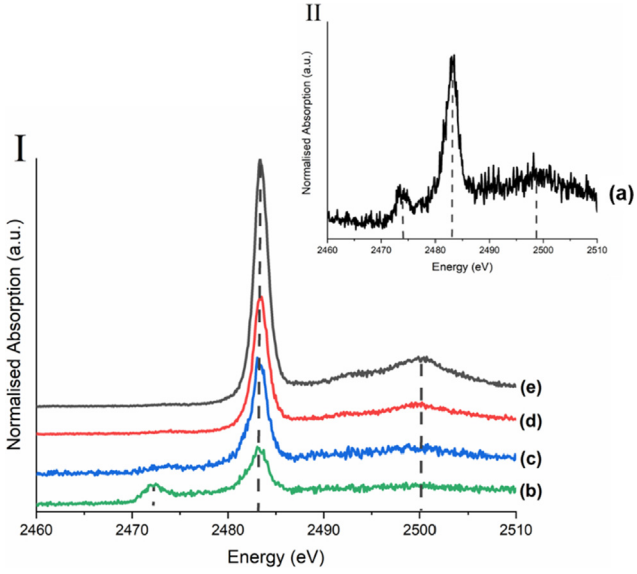

Fig. 8. The sulfur K-edge of promoted pre-reaction samples with a fixed level of sodium (~2000 ppm) and varying sulfur concentration (b) 50 (c) 100 (d) 175 (e) 250 ppm. The profiles are vertically off-set for clarity. (II) (a) Displays sample Fe-Na-S_{10} on a reduced y axis scale.

Table 3
XANES data for reference materials ($FeSO_4$, Na_2SO_3, S, $Na_2S_2O_3$, FeS_2) detailing peak positions and formal oxidation state of the sulfur within the compound [42,43].

Reference Material	Peak Position (eV)	Formal oxidation state of sulfur
Iron sulfate ($FeSO_4$)	2483	+6
Sodium sulfite (Na_2SO_3)	2482	+4
	2479	
Sodium thiosulfate ($Na_2S_2O_3$)	2481	+2
	2472	
Elemental sulfur (S)	2473	0
Iron sulfide (FeS_2)	2483	−2
	2472	

3.6. INS reactor measurements, ambient pressure CO hydrogenation at 623 K

Fig. 10 presents the post-reaction INS spectra recorded at incident energies of 650 and 250 meV for the five doubly promoted iron catalysts: Fig. 10**(I)** covers the range 2500–3750 cm^{-1}; Fig. 10**(II)** covers the range 400–1500 cm^{-1}. The signal intensity in Fig. 10 is inferior to that reported for **Fe-ref** [30], indicating a lower degree of hydrogen retention with this series of samples. Inspection of the C-H stretching region (2400–3750 cm^{-1}) presented in Fig. 10**(I)**, reveals the presence of hydrocarbon ν (C-H) moieties, with a prominent sp^2 hybridised carbon feature at 3048 cm^{-1} and a lower frequency sp^3 hybridised carbon shoulder at 2932 cm^{-1} [27–33]. Importantly, there is a clear decline in the formation of a hydrocarbonaceous overlayer on increasing S content. However, one sample, **Fe-Na-S_{100}**, lies out with this trend; this is attributed to the higher level of sodium associated with this sample (Table 1).

Adopting calibration procedures that exploit the quantitative features of INS spectroscopy [41], Fig. 11 presents the hydrogen content for the aliphatic and aromatic-olefinic C-H stretching modes as a function of S concentration. For comparative purposes, **Fe-ref** data corresponding to a 6 h CO hydrogenation run [30] are included in the figure. The incorporation of only 10 ppm of sulfur leads to a sharp reduction in intensity of the sp^3 hybridised feature

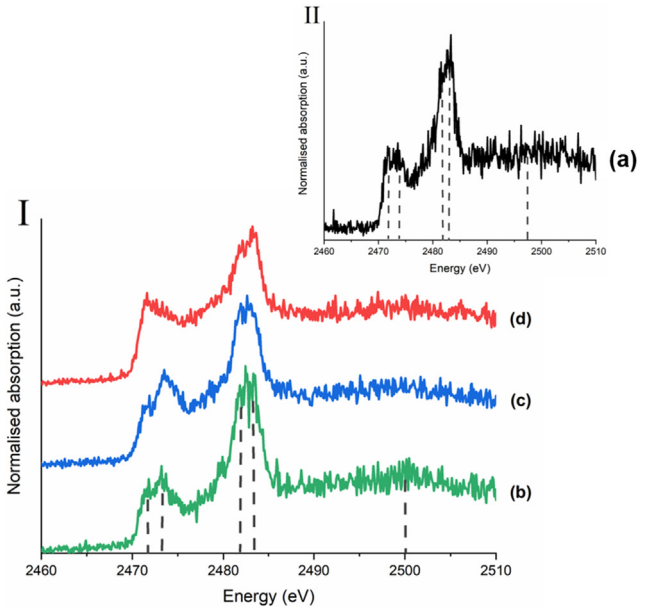

Fig. 9. The sulfur K-edge of each of the doubly promoted samples after exposure to ambient pressure CO hydrogenation conditions in the micro-reactor at 623 K for 6 h, with a fixed level of sodium (2000 ppm) and varying sulfur concentration (b) 50 (c) 100 (d) 175 ppm S. The profiles are vertically off-set for clarity. (II) (a) Displays sample Fe-Na-S_{10} post-reaction on a reduced y axis scale.

to almost baseline levels, that is maintained as the S concentration is increased. The decrease is less dramatic for the sp^2 hybridised feature although by 250 ppm of S it too is approaching baseline intensities. Fig. 11 indicates a degree of differentiation between how increasing S content quenches the two identifiable components of the hydrocarbonaceous overlayer. The slight 'blip' in the trend line for the sp^2 hybridised ν (C-H) feature at 100 ppm S is attributed to the larger Na value for this sample (Section 3.1).

The deformation region of the INS spectra (400–1600 cm^{-1}) are presented in Fig. 10**(II)** that shows the presence of weak and predominately aromatic components for all samples except **Fe-Na-S_{250}**. The specific assignments of these features include (i) a C-C torsion mode of edge carbon atoms contained within a polycyclic aromatic network (506 cm^{-1}) [46], (ii) an out-of-plane C-H deformation of either an olefinic or aromatic group (871 cm^{-1}) [47], (iii) a CC-H in plane deformation of a polyaromatic hydrocarbon (1160 cm^{-1}), (iv) a semi-circle ring deformation mode that may be linked to a δ(C-H) mode associated with carbons on the perimeter of an extended polyaromatic network (1451 cm^{-1}) [31,46], and (v) an alkenic δ(C-H) (953 cm^{-1}) [27–33,48]. It is noted that the sample containing the highest sulfur loading (**Fe-Na-S_{250}**) exhibits a slightly different deformation spectrum to that observed for the lower S concentrations, with peaks displayed at 541 and 941 cm^{-1} that are respectively assigned to the A_{1g} Fe-O phonon mode of Fe_3O_4 and a combination of alkenic δ(C-H) and a magnetic interaction associated with Fe_3O_4 [27–33,48]. Thus, in concert with the higher frequency spectra (Fig. 10**(I)**), this low frequency spectrum for the high S dosage sample (Fig. 10**(II)e**) shows minimal contribution from hydrocarbonaceous species and, instead, is characterised by magnetite derived magnon (spinon) features [31]. On initial inspection this seems contradictory to the post-reaction XRD results that show uniquely iron carbide formation (Fig. 7). However, as discussed elsewhere [31], for equivalent durations of time-on-stream, the reaction coordinate is significantly more advanced in the micro-reactor measurements compared to that experienced in the INS experiments that, for sensitivity reasons,

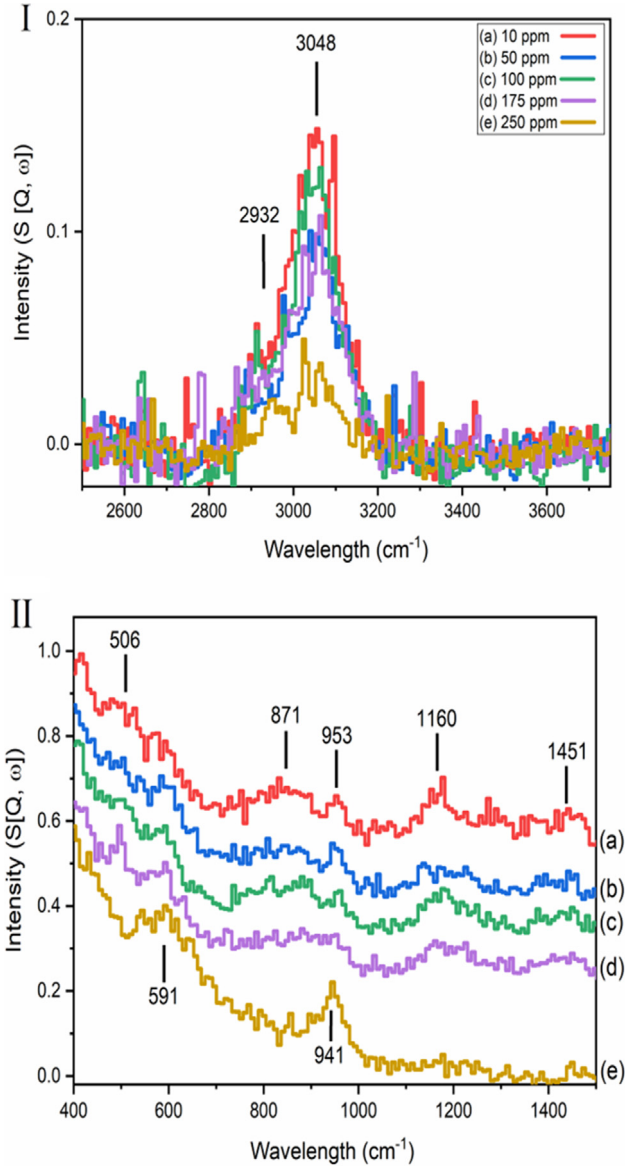

Fig. 10. INS spectra of Na/S promoted α-Fe_2O_3 (Na ~ 2000 ppm and varying sulfur concentrations (a) 10, (b) 50, (c) 100, (d) 175 and (e) 250 ppm) after CO hydrogenation at 623 K for 8 h in the INS reactor recorded at (I) 650 meV and (II) 250 meV. (II) is offset for clarity.

are operated at a relatively lower space velocity due to the larger catalyst charge requirement of the INS measurement.

4. Discussion

The elevated pressure reaction testing data of Table 2 shows that solely sodium doping at a level of ~2000 ppm leads to an increase in low molecular weight olefin selectivity and a reduction in methane formation. It also shows that the Na/S promoted samples over a sulfur range of 10–100 ppm do not disrupt the sodium induced changes in product distribution. However, Fig. 3 shows that sulfur concentrations > 100 ppm lead to significant improvements of C_2-C_4 olefin selectivity. At a sulfur concentration of 250 ppm this corresponds to an olefin selectivity value of 35.2%. Therefore, in the presence of sodium, Fig. 3 identifies the threshold sulfur concentration necessary to induce observed enhanced olefinicity. This outcome is thought to connect with the work of Bromfield and Coville, who reported a peak in specific activity for

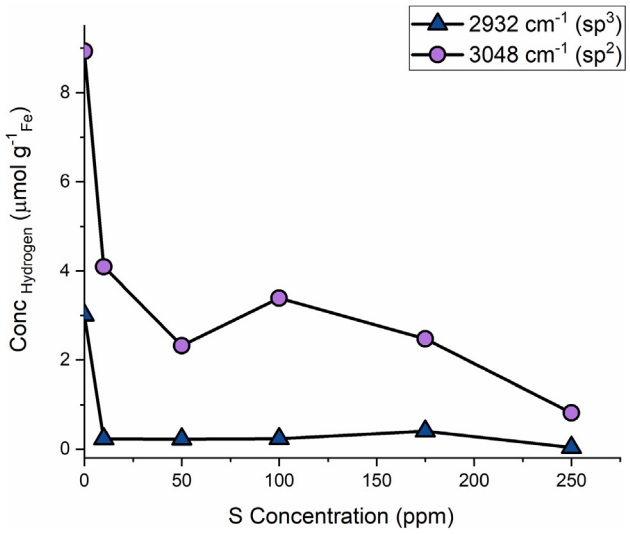

Fig. 11. Hydrogen content (μmol g^{-1}_{Fe}) of the ν(C-H) modes 2932 cm^{-1} (triangles) and 3948 cm^{-1} (circles) after exposure to CO hydrogenation conditions at 623 K for 8 h. For comparative purposes between promoted and unpromoted samples, Fe-ref values are included that correspond to the same reaction conditions but for 6 h duration [30].

a range of sulfided iron catalysts at a sulfur concentration of 500 ppm [18].

XRD of the doubly promoted pre-catalysts shows no deviation in structure compared to the unpromoted reference catalyst (Fig. 1) and S K-edge XANES measurements show the sulfur to be predominantly present as S^{6+} (Fig. 8). Linking these outcomes to the observation that the surface area and pore volumes are comparable to that of the unpromoted reference catalyst (Table 1), indicates that the promoter addition process over the concentration range studied has minimal effect on the pre-catalyst structure, with the S predominantly retained throughout the network as a sulfate anion.

TPR measurements show the increasing sulfur concentration to shift the reduction temperature of the hematite pre-catalyst to higher temperatures (Fig. 2). This attribute manifests itself in the ambient pressure CO hydrogenation profiles, whereby extended periods of CO_2 production at the higher S concentrations are observed (Fig. 4). These outcomes signify the sulfur to be exhibiting a mild chemical effect, whilst not inducing significant structural changes.

Post-reaction TPO measurements show excessive carbon retention for the Na/S doped samples compared to that previously reported for the unpromoted iron oxide reference catalyst (Fig. 5). As previous measurements on solely S promoted iron catalysts similarly exhibit increased carbon retention levels [33], the S is thought to be a significant contributor here. A relatively enhanced contribution of the transitive α feature in the carbon TPO profiles observed in Figs. 5 and 6 is thought to be associated with a chemically induced constraint of the global catalyst conditioning process, which manifests itself as a relatively enhanced concentration of the carbon α TPO feature at the catalyst surface.

Water signals in the TPO measurements show low levels of hydrogen to be associated with the α and β features that exhibit a small increase in intensity on increasing S concentration (Fig. 6**II**). However, a high temperature shoulder of the γ peak shows a modest but progressive attenuation as the S concentration is increased. Recent work from this group has refined the assignment for the carbon-derived TPO profiles, with the γ feature attributed to iron carbide entities plus polyaromatic carbonaceous species [32]. It is possible that the S could be systematically reducing the presence of polyaromatic carbonaceous species at the catalyst surface. This links in with the INS measurements that show the formation of a hydrocarbonaceous overlayer to be remarkably sensitive to sulfur concentration (Fig. 11). Interestingly, the sp^3 and sp^2 hybridised C-H components of the overlayer exhibit different sensitivities that do not directly match with the low molecular weight olefin selectivity profile presented in Fig. 3. As the sp^3 hybridised ν (C-H) mode is selectively suppressed at just 10 ppm, this component is not thought to be influential in enhancing olefin selectivity. More relevant perhaps is the matter of the sp^2 hybridised ν (C-H) mode that exhibits a progressive decrease in intensity in the 100–250 ppm region that corresponds to the enhanced olefin selectivity noted in Fig. 3. Consequences of this perspective will be developed further below.

XRD analysis of the post-reaction doubly promoted samples show uniquely iron carbide formation over the full range of S values (Fig. 7). Based on previous measurements [31,32], the carbide is attributed to Hägg carbide, which is thought to define the active phase of the working catalyst [31]. Paalanen *et al.* have recently used the techniques of XRD and Raman spectroscopy to examine the role of iron carbide and carbon species in Na/S promoted alumina-supported iron catalysts that display favourable C_2-C_4 olefin content [12]. The work shows considerable complexity concerning how Na/S promotion can alter the form of the iron carbide phase and the nature of the retained carbon [12]. However, with reference to Fig. 7, the fact that the iron carbide diffraction pattern is invariant to sulfur coverages, which Fig. 3 shows to favourably influence olefin yields, suggest that, in this case, the sulfur is not significantly perturbing the iron carbide structure over the range of sulfur values studied. On the other hand, S K-edge XANES measurements of the post-reaction micro-reactor samples (Fig. 9) show reduced levels of sulfur, with the sulfur present in a range of oxidation states (S^{6+}, S^{4+} and S^{2-}). This distribution of oxidation states is thought to reflect a progressive reduction process under reaction conditions. It is noted that the low sulfur levels responsible for inducing higher olefin selectivity (Fig. 3) constitute a challenge in terms of chemical and spatial identification of the counter ion. It is unfortunate that the S moieties were below the detection limit of the attempted TEM/EELS measurements on the pre-catalysts (Section 3.1).

The addition of Na and S as co-modifiers to a reference iron-based FTS catalyst to induce FTO activity is expected to add further complexity to the already intricate physical and chemical properties of conventional FTS catalysis [31,32]. Table 2 and Fig. 3 indicate favourable macroscopic benefits in terms of olefin selectivity for sulfur concentrations of $\geq$ 100 ppm. The fact that Fig. 2 shows the reduction profile for the Fe-ref sample to shift to higher temperatures from sulfur levels as low as 10 ppm suggests that the catalyst experiences the effect of the sulfur addition at this concentration but that its influence is small and insufficient to affect the product analytical measurements. However, as considered above, Fig. 11 shows the extent and form of the hydrocarbonaceous overlayer to be selectively attenuated over the 10–250 ppm concentration range; indicating a sensitivity for this molecular parameter over and above that obtainable in the elevated pressure reaction testing measurements.

The authors have previously suggested that the hydrocarbonaceous overlayer plays a role in facilitating hydrogen supply to the active sites (as defined by a partially masked Hägg carbide [31]), with a reduced hydrogen supply limiting both hydrogenation and C-C propagation steps of the FTS process [31]. Figs 10 and 11 show increasing concentration of S species restricts the formation of the overlayer. The reduced methane formation evident in Table 2 is consistent with this postulate of a catalytic system experiencing a constrained supply of surface hydrogen atoms. It is thought that this regulation of the surface supply of hydrogen relative to carbon has the same net effect that is provided by sodium, which

enhances the supply of carbon via facile CO dissociation. This scenario potentially provides an explanation for why dual promotion is more amenable for inducing FTO surface chemistry [6,24].

Overall, the multi-technique, multi-reactor approach has provided new insight into the complexity surrounding efficient FTO catalysis. It is clearly not a single phenomenon event; rather, it requires an inter-dependency of various parameters operating in a phased manner. Reflecting the inherent dynamics of this multivariate catalytic process [31,32], the temporal dependence of the hydrocarbonaceous overlayer and associated partner processes could be usefully explored. That aspiration constitutes 'work in progress'.

5. Conclusions

Following confirmation by high pressure reaction testing of the viability of the unpromoted iron oxide as a representative FTS catalyst and the Na/S-promoted materials as representative FTO catalysts, these samples have been further investigated. Utilising ambient pressure CO hydrogenation as a test reaction in INS and micro-reactor configurations, the samples have been analysed by TPR, XRD, TPO and XANES. The following conclusions can be drawn.

- XRD of the doubly promoted pre-catalysts show no deviation in structure compared to the unpromoted reference catalyst. S K-edge XANES measurements of the pre-catalysts show the sulfur to be predominantly present as the sulfate anion.
- TPR measurements show that increasing sulfur concentration shifts the reduction temperature of the hematite pre-catalyst to higher temperatures. This attribute manifests itself in the ambient pressure CO hydrogenation profiles by extended periods of CO_2 production at the higher S concentrations.
- Post-reaction TPO measurements show excessive carbon retention for the Na/S doped samples compared to that previously reported for the unpromoted iron oxide reference catalyst. A relatively enhanced contribution of the transitive α feature in the TPO profiles is thought to be an indication of a chemically induced constraint of the global catalyst conditioning process.
- S K-edge XANES measurements of the post-reaction micro-reactor samples shows the presence of a range of oxidation states (S^{6+}, S^{4+} and S^{2-}). This distribution is thought to reflect a progressive reduction process under reaction conditions.
- INS shows formation of the hydrocarbonaceous overlayer to be significantly attenuated by the presence of the promoters, with increasing S values reducing the intensity of the ν (C-H) modes of the overlayer.
- The hydrocarbonaceous overlayer has been postulated to play a role in facilitating hydrogen supply to active sites and its attenuation by S provides a plausible mechanism for the observed shifts towards olefin selectivity. Sulfur and sodium are thought to operate in unison by regulating the supply of hydrogen and carbon respectively to promote the formation of unsaturated products.

Declaration of Competing Interest

The authors declare that they have no known competing financial interests or personal relationships that could have appeared to influence the work reported in this paper.

Acknowledgements

Sasol Ltd., the University of Glasgow and EPSRC [award reference EP/P505534/1.] are thanked for the provision of postgraduate studentship (ALD). The STFC Rutherford Appleton Laboratory is thanked for access to neutron beam facilities [RB 1520269/1610413]. Diamond Light Source is thanked for time on B18 beamline through the Catalysis Hub BAG application (SP15151 and rapid access beamtime SP18431). The Royal Society is thanked for the provision of an Industry Fellowship (PBW).

Appendix A. Supplementary material

Supplementary data to this article can be found online at https://doi.org/10.1016/j.jcat.2020.09.025.

References

[1] J. Schneider, M. Struve, U. Trommler, M. Schlüter, L. Seidel, S. Dietrich, S. Rönsch, Fuel Process. Technol. 170 (2018) 64–78.
[2] J. Van de Loosdrecht , F.G. Botes, I.M. Ciobica, A. Ferreira, P. Gibson, D.J. Moodley, A.M. Saib, J.L. Visage, C.J. Weststrate, J.W. Niemantsverdriet, in Fischer-Tropsch Synthesis: Catalysts and Chemistry. In: Comprehensive Inorganic Chemistry II, Elsevier, Oxford, 2013, vol. 7, pp. 525–557.
[3] A.P. Steynberg, M. Dry, Fischer-Tropsch Technology, Elsevier, 2004.
[4] G.F. Botes, T.C. Bromfield, R.L.J. Coetzer, R. Crous, P. Gibson, A.C. Ferreira, Catal. Today 275 (2016) 40–48.
[5] Y. Yuan, S. Huang, H. Wang, Y. Wang, J. Wang, J. Lv, Z. Li, X. Ma, ChemCatChem 9 (2017) 3088–3089.
[6] H.M. Torres Galvis, A.C.J. Koeken, J.H. Bitter, T. Davidian, M. Ruitenbeek, A.I. Dugulan, K.P. de Jong, J. Catal. 303 (2013) 22–30.
[7] H.M. Torres Galvis, A.C.J. Koeken, J.H. Bitter, T. Davidian, M. Ruitenbeek, A.I. Dugulan, K.P. De Jong, Catal. Today 215 (2013) 95–102.
[8] H.M. Torres Galvis, K.P. De Jong, ACS Catal. 3 (2013) 2130–2149.
[9] F. Jiang, M. Zhang, B. Liu, Y. Xu, X. Liu, Catal, Sci. Technol. 7 (2017) 1245–1265.
[10] A.J. McCue, J.A. Anderson, Catal. Sci. Technol 4 (2014) 272–294.
[11] P.P. Paalanen, B.M. Weckhuysen, ChemCatChem 12 (2020) 1–23.
[12] P.P. Paalanen, S.H. van Vreeswijk, B.M. Weckhuysen, ACS Catal. 10 (2020) 9937–19855.
[13] P.P. Paalanen, S.H. van Creeswijk, A.I. Dugulan, B.M. Wechhuysen, ChemCatChem (2020), https://doi.org/10.1002/cctc.202000707.
[14] F. Jiao, J. Li, X. Pan, J. Xiao, H. Li, H. Ma, M. Wei, Y. Pan, Z. Zhou, M. Li, S. Miao, J. Li, Y. Zhu, D. Xiao, T. He, J. Yang, F. Qi, Q. Fu, Z. Bao, Science 351 (2016) 1065–1068.
[15] X. Zhou, J. Ji, D. Wang, X. Duan, G. Qian, D. Chen, X. Zhou, Chem. Commun. 51 (2015) 8853–8856.
[16] Y. Cheng, J. Lin, K. Xu, H. Wang, X. Yao, Y. Pei, S. Yan, M. Qiao, B. Zong, ACS Catal. 6 (2016) 389–399.
[17] Y. Zhu, X. Pan, F. Jiao, J. Li, J. Yang, M. Ding, Y. Han, Z. Liu, X. Bao, ACS Catal 7 (2017) 2800–2804.
[18] T.C. Bromfield, N.J. Coville, Appl. Catal. A Gen. 186 (1999) 297–307.
[19] M.C. Ribeiro, G. Jacobs, B.H. Davis, D.C. Cronauer, A.J. Kropf, C.L. Marshall, J. Phys. Chem. C 114 (2010) 7895–7903.
[20] J.W. Niemantsverdriet, A.M. van der Kraan, W.L. van Dijk, H.S. van der Baan, J. Phys. Chem. 84 (1980) 3363–3370.
[21] J.W. Niemantsverdriet, A.M. van der Kraan, J. Catal. 72 (1981) 385–388.
[22] M.E. Dry, J.C. Hoogendoorn, Catal. Rev. Eng. 23 (1981) 265–278.
[23] C.H. Bartholomew, R.M. Bowman, Appl. Catal. 15 (1985) 59–67.
[24] J.A. Kritzinger, Catal. Today 71 (2002) 307–318.
[25] R Crous, T.C. Bromfield, S. Booyens, Olefin selective FT catalyst composition and preparation thereof, Sasol Technology (Pty.) Ltd, South Africa, Patent PCT Int. Appl. WO 2010/066386 (2010).
[26] J. Xie, J. Yang, A.I. Dugulan, A. Holmen, D. Chen, K.P. De Jong, M.J. Louwerse, ACS Catal. 6 (2016) 3147–3157.
[27] N.G. Hamilton, I.P. Silverwood, R. Warringham, J. Kapitán, L. Hecht, P.B. Webb, R.P. Tooze, S.F. Parker, D. Lennon, Angew. Chem. Int. Ed. 52 (2013) 5608.
[28] N.G. Hamilton, R. Warringham, I.P. Silverwood, J. Kapitán, L. Hecht, P.B. Webb, R.P. Tooze, W. Zhou, C.D. Frost, S.F. Parker, D. Lennon, J. Catal. 312 (2014) 221–231.
[29] R. Warringham, N.G. Hamilton, I.P. Silverwood, C. How, P.B. Webb, R.P. Tooze, W. Zhou, C.D. Frost, S.F. Parker, D. Lennon, Appl. Catal., A. 489 (2015) 209–217.
[30] R. Warringham, A.R. McFarlane, P.B. Webb, R.P. Tooze, J. Taylor, D.A. MacLaren, R. Ewings, S.F. Parker, D. Lennon, J. Chem. Phys. 143 (2015) 174703.
[31] R. Warringham, A.L. Davidson, P.B. Webb, R.P. Tooze, R.A. Ewings, S.F. Parker, D. Lennon, RSC Adv. 9 (2019) 2608–2617.
[32] A.L. Davidson, P.B. Webb, S.F. Parker, D. Lennon, Ind. Eng. Chem. Res. 59 (2020) 52–60.
[33] R. Warringham, A.L. Davidson, P.B. Webb, R.P. Tooze, S.F. Parker, D. Lennon, Catal. Today 339 (2020) 32–39.
[34] P.W. Albers, D. Lennon, S.F. Parker, in: Neutron Scattering - Applications in Biology, Chemistry, and Materials Science, ed. F. Fernandez-Alonso and D.L. Price, Academic Press, 2017, ch.5 Catalysis, pp. 279–348.
[35] S.F. Parker, D. Lennon, P.W. Albers, App. Spectrosc. 65 (2011) 1325–1341.
[36] M.D. Shroff, A.K. Dayte, Catal. Lett. 37 (1996) 101–106.

[37] I.P. Silverwood, N.G. Hamilton, A.R. McFarlane, J. Kapitan, L. Hecht, E.L. Norris, R.M. Ormerod, C.D. Frost, S.F. Parker, D. Lennon, Phys. Chem. Chem. Phys. 14 (2012) 15214–15225.
[38] B. Ravel, M. Newville, J. Synchrotron Radiat. 12 (2005) 537–541.
[39] M. Newville, J. Synchrotron Radiat. 8 (2001) 322–324.
[40] R. Warringham, D. Bellaire, S.F. Parker, J. Taylor, R.A. Ewings, C.M. Goodway, M. Kibble, S.R. Wakefield, M. Jura, M.P. Dudman, R.P. Tooze, P.B. Webb, D. Lennon, J. Phys.: Conf. Ser., 2014, 554, 012005.
[41] I.P. Silverwood, N.G. Hamilton, C.J. Laycock, J.Z. Staniforth, R.M. Ormerod, C.D. Frost, S.F. Parker, D. Lennon, Phys. Chem. Chem. Phys. 12 (2010) 3102–3107.
[42] F. Farges, P. Lens, M. Lenz, S. Rossano, J. Labanowski, A.-M. Flank, E. van Hullebusch, P. Lagarde, J. Phys. Conf. Ser. 190 (2009) 012184.
[43] J. Evans, X-ray Absorption Spectroscopy for the Chemical and Material Sciences, Wiley, 2018.
[44] J.E. Penner-Hahn, Comprehensive Coordination Chemistry II, Volume 2, ed. J. A. MCCleverty and T. J. Meyer, Elsevier Ltd., 2nd ed., 2003, ch.2.13, pp. 159–186.
[45] T.C. Bromfield, N.J. Coville, Appl. Surf. Sci. 119 (1997) 19–24.
[46] P.W. Albers, J. Pietsch, J. Krauter, S.F. Parker, Phys. Chem. Chem. Phys. 5 (2003) 1941–1949.
[47] D. Lin-Vien, N.B. Colthup, W.G. Fateley, J.G. Graselli, The handbook of infrared and Raman characteristic frequencies of organic molecules, Academic Press, Boston, 1991.
[48] I. Chamritski, G. Burns, J. Phys. Chem. B 109 (2005) 4965–4968.